RESEARCH ARTICLE
doi: 10.2306/scienceasia1513-1874.2020.002

*ScienceAsia* 46 (2020): **46–51**

# $Yb^{3+}/Er^{3+}$ concentration dependent microstructure evolution and green/red emissions of $NaYF_4$:Yb/Er phosphors

**Yanli Ding**[a,b,*], **Tonghui Yang**[a], **Naiqiang Yin**[a], **Peng Li**[a], **Ying Zhao**[b], **Xiaodan Zhang**[b]

[a] School of Electrical and Electronic Engineering, Shangqiu Normal University, Shangqiu 476000 China
[b] Institute of Photo-electronic Thin Film Devices and Technology, Nankai University, Tianjin 300071 China

*Corresponding author, e-mail: yanliding2006@163.com

*Received 16 Feb 2019*
*Accepted 22 Dec 2019*

**ABSTRACT**: Photon upconversion is promising for applications such as data storage, drug delivery and solar cells. β-$NaYF_4$:Yb/Er samples were synthesized by a facile hydrothermal method. The effects of Yb/Er ratio on the microstructures, morphology evolution and luminescence properties were studied. The SEM results showed that the morphology of the samples evolved gradually from plate to prismatic structure with an increase in $Yb^{3+}$ concentration. This indicates that the growth rate along the c-axis crystal planes of $NaYbF_4$ lattices is more rapid than $NaYF_4$ lattices. Photoluminescence measurements demonstrate that the bright multicolored upconversion emissions can be fine-tuned from green to red by adjusting the codoped Yb/Er ratio under 980 nm laser excitation. The tunable emission is due to the energy back transfer from $Yb^{3+}$ to $Er^{3+}$. Applying this material in perovskite solar cell, a current density of 4 μA $cm^{-2}$ is obtained under 40 mW and 980 nm laser excitation.

**KEYWORDS**: upconversion, Yb/Er ratio, hydrothermal method, perovskite solar cell

## INTRODUCTION

Lanthanide-doped upconversion (UC) phosphors have received considerable attention in recent years because of their unique ability to generate high energy photons under low energy photon excitations [1]. These unique anti-Stokes emitters have opened up the opportunity for applications in diverse fields such as sensors [2], solar cells [3] and fluorescent probes for bioimaging [4, 5]. However, different applications have different requirements for their light emission. Compared with conventional fluorescent probes materials, upconversion phosphors show great advantages due to the low toxicity, minimal low background light, high penetration depth and minimum photodamage to biological tissues [6, 7]. As is known, the red emission is preferred to be used as a probe for *in vivo* imaging since the red emission could afford the deeper tissue penetration than the green emission [8]. Therefore, rational controlling the two emissions output in order to effectively avoid the generation of short-wavelength green emission and enhance the red emission output of Yb/Er codoped $NaYF_4$ nanoparticles is important for their application *in vivo* imaging. In addition, perovskite solar cells (PSC) can only utilize a small portion of the solar spectrum (400–800 nm) due to the limited of the bandgap (1.55 eV), leading to an energy loss of near infrared (NIR) light. One promising way to solve this problem is to use upconversion materials as spectral converters [3]. Guo and Roh have introduced upconversion materials to the $TiO_2$ mesoporous layer in a PSC device for NIR sunlight harvesting [9, 10].

In this work, the microstructures, morphology evolution and UC fluorescence properties of $NaYF_4$:Yb/Er with different Yb/Er ratio were investigated. Placing this material in hole-transfer layer of perovskite solar cell, the short-circuit current densities were measured.

## MATERIALS AND METHODS

All the chemical reagents used in this experiment are analytical grade without further purification. $YCl_3 \cdot 6H_2O$ (99.99%), $Yb_2O_3$ (99.99%), $Er_2O_3$ (99.99%), NaCl (99.95%), $NH_4F$, ethanol and ethylenediamine tetraacetic acid (EDTA) were purchased from Tianjin Guangfu Fine Chemical Research Institute. Water used in the experiment was purified to a resistivity of 18.2 MΩ.

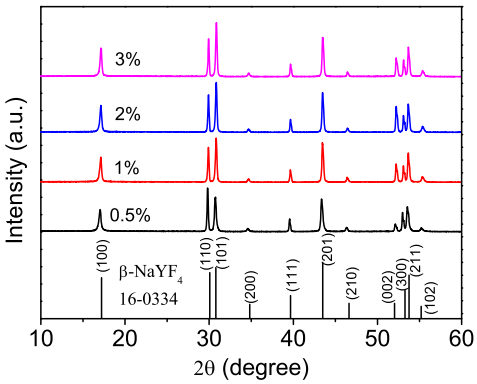


**Fig. 1** XRD patterns of $NaYF_4$:Yb 18%, Er $x$% ($x = 0.5, 1, 2, 3$).

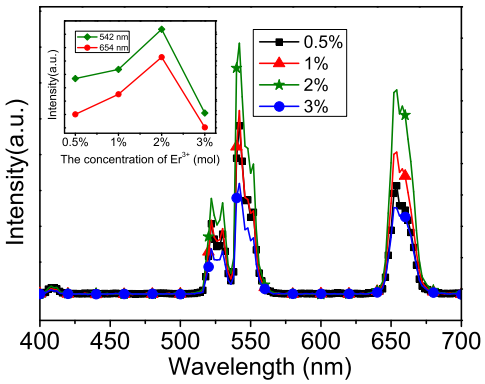


**Fig. 2** UC emission spectra of $NaYF_4$:Yb 18%, Er $x$% ($x = 0.5, 1, 2, 3$) under 980 nm diode laser excitation.

### Preparation of $NaYF_4$:Yb,Er microcrystals

$NaYF_4$:Yb,Er microcrystals were synthesized by a simple hydrothermal procedure [11]. In a typical process, $RECl_3$ (0.2 M, 15 ml) (RE = $Y^{3+}$, $Yb^{3+}$, $Er^{3+}$ and $Y^{3+}$:$Yb^{3+}$:$Er^{3+}$ = 49:9:1) and EDTA (0.2 M, 24 ml) aqueous solutions were mixed with 22.5 ml absolute ethanol under vigorous stirring. Subsequently, NaCl (0.2 M, 15 ml) and $NH_4F$ (0.56 g) were added into the above solution. The resulting mixture was transferred into a 100 ml stainless teflon-lined autoclave, which was sealed and heated at 200 °C for 24 h in an electric drying oven. The reaction mixture was precipitated via centrifuging, the precipitate was washed with deionized water and ethanol several times and vacuum dried at 80 °C for 8 h.

X-ray diffraction (XRD) analysis was performed on a Rikaku, ATX-XRD with Cu Ka radiation ($\lambda$ = 1.5405 Å) in the 2θ range from 10–80°. The morphology of the samples was obtained using a Jeol JSM-6700F scanning electron microscopy (SEM). The UC emission spectra of the powder samples were measured on a Fluorolog-3 luminescence spectrometer under a 980 nm laser excitation with a power of 40 mW, the power density is 0.04 W/mm$^2$. The $NaYF_4$:Yb,Er particles were blended into a spiro-OMeTAD solution and spin-coated on top of the perovskite layer as the hole-transfer layer. Finally, the devices were completed by thermal evaporation of 100 nm Au electrode. The photocurrent density of perovskite solar cells without and with $NaYF_4$:Yb,Er particles were measured under 980 nm laser excitation.

## RESULTS

In order to obtain highly efficient luminescent materials, doped activated ions need a suitable concentration. Fig. 1 presents the XRD patterns of $NaYF_4$ doped with 18 mol% Yb/$x$ mol% Er ($x$ = 0.5, 1, 2, 3). It can be seen that all diffraction peaks can be indexed in accordance with hexagonal-phase $NaYF_4$ crystals (JCPDS card 16-0334), indicating the formation of pure hexagonal-phase.

Fig. 2 shows the UC emission of $NaYF_4$ doped with 18 mol% Yb/$x$ mol% Er ($x = 0.5, 1, 2, 3$). As illustrated in Fig. 2, these emission spectra display two strong emission bands of approximately equal intensity in the green (540 nm) and red (652 nm), a weak emission bands in the green (525 nm), corresponding to $^4S_{3/2} \rightarrow {}^4I_{15/2}$, $^4F_{9/2} \rightarrow {}^4I_{15/2}$ and $^2H_{11/2} \rightarrow {}^4I_{15/2}$ electronic transition, respectively. A much weaker violet emission at 407 nm is observed and attributed to the $^2H_{9/2} \rightarrow {}^4I_{15/2}$ electronic transition. It can be seen that different doping concentration leads to the differences of relative intensities of each emission peak. The highest intensities of the green and red emissions are observed at 2 mol%. As the doping concentration of $Er^{3+}$ increases, both green and red emission intensities of the samples decrease. It is also well-known that a high doping level can lead to deleterious resonant energy transfer, the distance between $Er^{3+}$—$Er^{3+}$ becomes close that the concentration quenching is obvious, leading to the intensity dropping down [12].

Fig. 3a presents the XRD patterns for $NaYF_4$ doped with 2 mol% Er/$y$ mol% Yb ($y$ = 15, 18, 25, 98). All powder samples are hexagonal structure according to Powder Diffraction File PDF 16-0334. To reveal the subtle differences

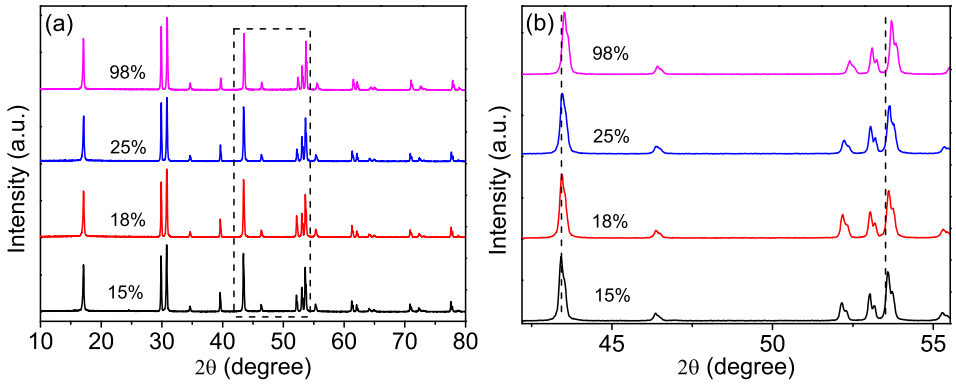


**Fig. 3** (a) XRD patterns of $NaYF_4$ doped with different $Yb^{3+}$ ion concentrations. (b) Diffraction peak shift as the function of $Yb^{3+}$ ion concentrations.

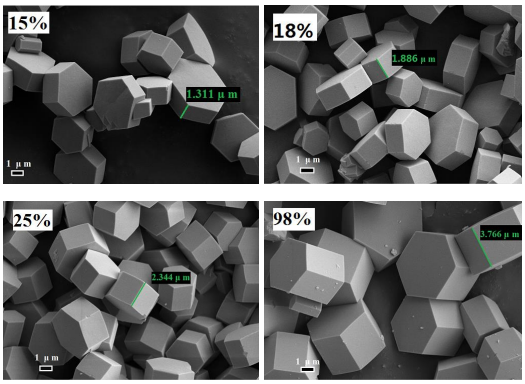


**Fig. 4** SEM images of the $NaYF_4$ doped with different $Yb^{3+}$ ion concentrations.

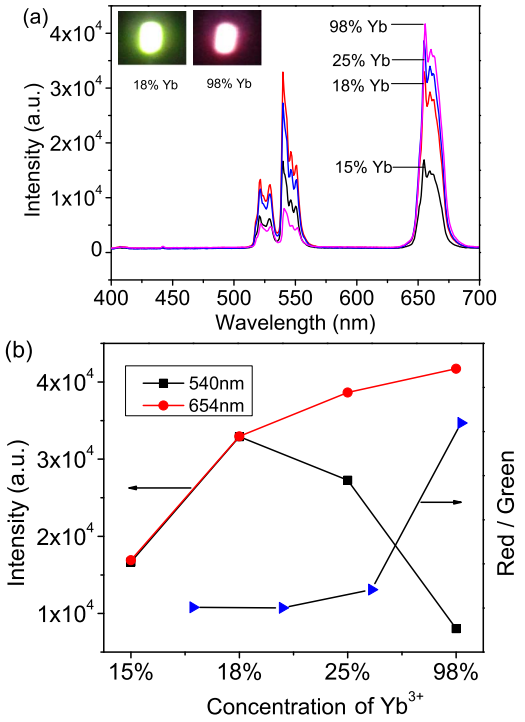


**Fig. 5** (a) UC emission of $NaYF_4$ doped with 2 mol% Er/$y$ mol% Yb ($y = 15, 18, 25, 98$). The inset is the luminescent photograph of $NaYF_4$:18% Yb, 2% Er and $NaYF_4$:98% Yb, 2% Er under the excitation of 980 nm. (b) The intensity of red, green emission and the red/green ratio as a function of $Yb^{3+}$ concentrations.

caused by the increase of $Yb^{3+}$ ion concentrations, a selected region of diffraction peaks was magnified and shown in the Fig. 3b. As can be seen clearly, a slight shift of peaks to high 2θ angle can be observed due to the increase of $Yb^{3+}$ ion concentrations. This may be caused by the substitution of $Y^{3+}$ ions (radius: 0.89 Å) by smaller $Yb^{3+}$ ions (radius: 0.86 Å) in the host lattice.

To confirm the result, the SEM images of the $NaYF_4$ doped with different $Yb^{3+}$ ion concentrations are shown in Fig. 4. It can be seen that the size and morphology of samples are hexagonal microplates. When $Yb^{3+}$ ion concentration increases from 15% to 18%, 25%, and 98%, respectively, the thickness of microplates are increased from 1.311 μm to 1.866 μm, 2.344 μm, and 3.766 μm. The morphology of the samples evolved gradually from plate to prismatic structure. This indicates that the growth rate along the c-axis crystal planes of $NaYbF_4$ lattices is more rapid than $NaYF_4$ lattices.

The difference of crystal structure and morphology usually leads to the change of the luminescence properties. Fig. 5a shows the UC emission of $NaYF_4$ doped with 2 mol Er%/$y$ mol% Yb ($y = 15, 18, 25, 98$). It can be seen that the intensity of

green emission first rises up to the maximum at 18 mol% $Yb^{3+}$ and then decreases with further increasing the concentration of $Yb^{3+}$ ion. While the emission intensity of red increases monotonously with the $Yb^{3+}$ concentration increase and the ratios of the red to green emission are consequently increased (Fig. 5b). When $Yb^{3+}$ ion concentration is 98%, as a result the samples exhibit bright red luminescence (inset of Fig. 5a). Compared with the green light, red light has less penetrating damage to biological tissue, so the monochromatic red light plays an important role in the application of fluorescence probe. According to above results, the UC emission intensity of each band is markedly dependent on the concentration of $Er^{3+}$ and $Yb^{3+}$ ions, and the effect of $Yb^{3+}$ ions is dominant. By tuning the doped $Yb^{3+}$ concentration we can precisely manipulate the relative emission intensities, thus resulting in a tunable color output from green to red. The color coordinates corresponding to the emission spectra of the samples doped with 18% $Yb^{3+}$ and 98% $Yb^{3+}$ have been calculated using suitable software. The CIE-1931 color coordinates $(x, y)$ are shown in Fig. 6a. The emission color changes from green to red by increasing $Yb^{3+}$ concentration. Such tunable luminescence is of interest for technical applications.

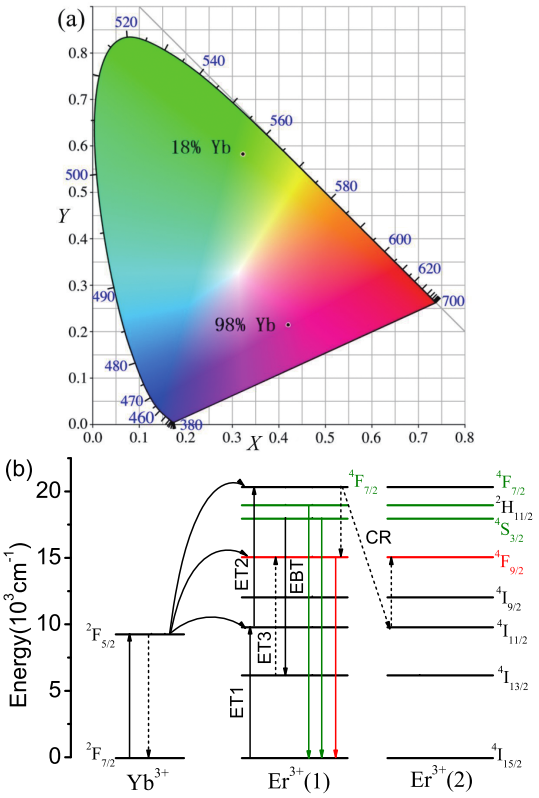


**Fig. 6** (a) CIE chromaticity diagram for the samples doped with 18% $Yb^{3+}$ and 98% $Yb^{3+}$. (b) Energy-level diagram of $Yb^{3+}/Er^{3+}$ co-doped UC materials and UC processes under 980 nm excitation.

## DISCUSSION

The mechanism of the change on the morphology can be partly attributed to the strong effect of the $Yb^{3+}$ ion concentration on crystal growth rate through surface charge modification. In the process of crystal growth, the density of $Y^{3+}$ on the six equivalent $\{10\bar{1}0\}$ families (a-axis) planes, consisting of $\pm\{1\bar{1}00\}$, $\pm\{01\bar{1}0\}$, and $\pm\{10\bar{1}0\}$ crystal planes, is higher than that on the typical top/bottom {0001} (c-axis) packing planes [13]. However, according to the first principle calculation of Wang et al, the electron charge density of the crystal surface should decrease after $Yb^{3+}$ ion substitutes $Y^{3+}$ ion in the crystal lattices [14]. Diffusion rate of the $F^-$ ions on the surface increases owing to the decreased charge repulsion. Subsequently, more superfluous $F^-$ ions capped the c-axis packing planes rather than the a-axis crystal planes due to the lower charge density, which inhibits the rate of the growth along the c-axis crystal planes [15], resulting in an increased speed of $NaYbF_4$ growth.

The detailed UC mechanism and population processes in $Er^{3+}$ and $Yb^{3+}$ co-doped systems are presented in Fig. 6b, which has also been described [16]. Two energy transfers, ET1 and ET2, from $Yb^{3+}$ ions can promote the $Er^{3+}$ ions to the $^4F_{7/2}$ level. The populated $^4F_{7/2}$ level can relax nonradiatively to the next lower $^2H_{11/2}$ and $^4S_{3/2}$ green emitting levels. Alternatively, the $Er^{3+}$ ion can further relax and populate the $^4F_{9/2}$ level, which leads to the red emission. At the higher doping concentration, the interatomic distance between $Er^{3+}$–$Er^{3+}$ or $Yb^{3+}$–$Er^{3+}$ decreases and further affects their UC emissions. There are two main possible pumping mechanisms for the population of the red emitting state. The first pumping mechanism is the energy back transfer (EBT) process [17]: $^4S_{3/2}(Er) + {}^2F_{7/2}(Yb) \rightarrow {}^4I_{13/2}(Er) + {}^2F_{5/2}(Yb)$. In the EBT process, the $^4F_{9/2} \rightarrow {}^4I_{13/2}$ upconversion mechanism is very efficient through ET3 and results in bypassing the green $^4S_{3/2}$ state. The second possible mechanism is the cross-relaxation (CR) process of $^4F_{7/2} + {}^4I_{11/2} \rightarrow {}^4F_{9/2} + {}^4F_{9/2}$. In two processes, the enhanced population of the $^4F_{9/2}$ state leads

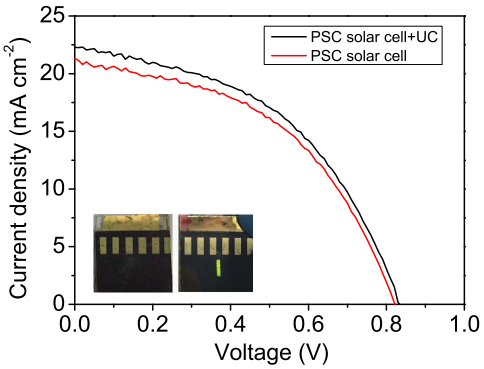


**Fig. 7** The pictures and the J-V characteristics of the perovskite solar cells fabricated without and with the UCPs.

**Table 1** Detailed photovoltaic parameters of the devices made without and with the $NaYF_4$:Yb,Er under one sun illumination at AM 1.5 G.

| Samples | $J_{SC}$ (mA cm$^{-2}$) | $V_{OC}$ (V) | *FF* | $\eta$ (%) |
|---|---|---|---|---|
| No UC | 21.31 | 0.817 | 47 | 8.2 |
| UC+Cell | 22.29 | 0.821 | 48 | 8.7 |

to a relative enhancement of the red emission and quenched the green emission.

In order to verify the effect of $NaYF_4$:Yb,Er, upconversion-perovskite solar cells were fabricated. 12 mg $NaYF_4$:Yb,Er powder were added into 1 ml spiro-OMeTAD solution and spin-coated on top of the perovskite layer as the hole-transfer layer (HTM). Finally, the devices were completed by thermal evaporation of 100 nm Au electrode. The pictures and photocurrent density-voltage (J-V) characteristics of the perovskite solar cells without and with the UCPs are shown in Fig. 7. The relative photovoltaic parameters are summarized in Table 1. The result indicates a 4.6% enhancement in $J_{SC}$ (from 21.31–22.29 mA cm$^{-2}$) compared with the pristine device, while $V_{OC}$ almost unchanged. The enhancement can be associated with the UC luminescence properties of UCNPs and enhanced scattering effect. To confirm the NIR response, the values of photocurrent density ($J_{SC}$) of solar cells were measured using a 40 mW and 980 nm NIR laser illumination. For the solar cell with no UCPs, no photovoltaic response exists due to the absence of the upconversion effect. However, the device made with 12 mg/ml UCPs in HTM exhibits a better photocurrent output of 4 μA cm$^{-2}$.

## CONCLUSION

In conclusions, we have systematically studied the effect of doping ratio on structure, morphology evolution and luminescent properties of β-$NaYF_4$:Yb/Er. The results showed that the morphology of the samples evolved gradually from plate to prismatic structure with an increase in $Yb^{3+}$ concentration, the intensity ratio of the green and red UC luminescence can be either increased or decreased conveniently by tuning the Yb/Er ratio. Applying this UC material in the HTM of perovskite solar cells, a current density of 4 μA cm$^{-2}$ is obtained under 40 mW and 980 nm laser excitation.

*Acknowledgements*: The authors gratefully acknowledge the supports from the National Natural Science Foundation of China (Grant No. 11704237, Grant No. U1704145), Henan Provincial Natural Science Foundation (192102210199, 182102410070), Henan Provincial Key Research Projects of Higher Education Institutions (20A140023).

## REFERENCES

1. Auzel F (2004) Upconversion and anti-stokes processes with f and d ions in solids. *Chem Rev* **104**, 139–173.
2. Ding MY, Zhang HL, Chen DQ, Hu QW, Xi JH, Ji ZG (2016) Color-tunable luminescence, energy transfer and temperature sensing behavior of hexagonal $NaYF_4$:$Ce^{3+}$/$Tb^{3+}$/$Eu^{3+}$ microcrystals. *J Alloy Compd* **672**, 117–124.
3. Day J, Senthilarasu S, Mallick JK (2019) Improving spectral modification for applications in solar cells: A review. *Renew Energy* **132**, 186–205.
4. Hu SG, Wu XF, Chen ZH, Hu P, Yan HY, Tang ZJ, Xi ZF, Liu YX (2016) Uniform NaLuF4 nanoparticles with strong upconversion luminescence for background-free imaging of plant cells and ultralow power detecting of trace organic dyes. *Mater Res Bull* **73**, 6–13.
5. Zhou J, Liu Z, Li FY (2012) Upconversion nanophosphors for small-animal imaging. *Chem Soc Rev* **41**, 1323–1349.
6. Lyu LN, Cheong HL, Ai XZ, Zhang WM, Li J, Yang HH, Lin J, Xing BG (2018) Near-infrared light-mediated rare-earth nanocrystals: recent advances in improving photon conversion and alleviating the thermal effect. *NPG Asia Mater* **10**, 685–702.
7. Yang YM, Mu J, Xing BG (2017) Photoactivated drug delivery and bioimaging. *WIREs Nanomed Nanobiotechnol* **9**, ID e1408.
8. Chen DQ, Lei L, Zhang R, Yang AP, Xu J, Wang YS (2012) Intrinsic single-band upconversion emission in colloidal Yb/Er(Tm):$Na_3Zr(Hf)F_7$ nanocrystals. *Chem Commun* **48**, 10630–10632.

9. Guo QY, Wu JH, Yang YQ, Liu XP, Jia JB, Dong J, Lan Z, Lin J, et al (2019) High performance perovskite solar cells based on β-$NaYF_4$:$Yb^{3+}$/$Er^{3+}$/$Sc^{3+}$ @$NaYF_4$ core-shell upconversion nanoparticles. *J Power Sources* **426**, 178–187.
10. Roh J, Yu H and Jang J (2016) Hexagonal β-$NaYF_4$:$Yb^{3+}$, $Er^{3+}$ nanoprism incorporated upconverting layer in perovskite solar cells for near-infrared sunlight harvesting. *ACS Appl Mater Interfaces* **8**, 19847–19852.
11. Ding YL, Zhang XD, Gao HB, Xu SZ, Wei CC, Zhao YJ (2014) Enhancement on concentration quenching threshold and upconversion luminescence of β-$NaYF_4$:$Er^{3+}$/$Yb^{3+}$ codoping with $Li^+$ ions. *J Alloys Comp* **599**, 60–64.
12. Zhang H, Li YJ, Lin YC, Huang Y, Duan XF (2011) Composition tuning the upconversion emission in $NaYF_4$:Yb/Tm hexaplate nanocrystals. *Nanoscale* **3**, 963–966.
13. Niu WB, Wu SL, Zhang SF, Li J, Li L (2011) Multicolor output and shape controlled synthesis of lanthanide-ion doped fluorides upconversion nanoparticles. *Dalton Trans* **40**, 3305–3314.
14. Wang F, Han Y, Lim CS, Lu YH, Wang J, Xu J, Chen HY, Zhang C, Hong MH, Liu XG (2010) Simulaneous phase and size control of upconversion nanocrystals through lanthanide doping. *Nature* **463**, 1061–1065.
15. Qin H, Wu DY, Sathian JN, Xie XY, Ryan M, Xie F (2018) Tuning the upconversion photoluminescence lifetimes of $NaYF_4$:$Yb^{3+}$, $Er^{3+}$ through lanthanide $Gd^{3+}$ doping. *Sci Rep* **8**, ID 12683.
16. Shan JN, Uddi M, Wei R, Yao N, Ju YG (2010) The hidden effects of particle shape and criteria for evaluating the upconversion luminescence of the lanthanide doped nanophosphors. *J Phys Chem C* **114**, 2452–2461.
17. Chen GY, Somesfalean G, Liu Y, Zhang ZQ, Sun Q, Wang FP (2007) Upconversion mechanism for two-color emission in rare-earth-ion-doped $ZrO_2$ nanocrystals. *Phys Rev B* **75**, ID 195204.